JOURNAL OF MATERIALS SCIENCE 27 (1992) 1642–1650

# Microstructures and mechanical properties of rapidly solidified niobium aluminide ($NbAl_3$)

RANJAN RAY
*Marko Materials, Inc., 19 Sterling Rd., North Billerica, MA 01862, USA*
RAGHAVAN AYER
*STEM, Inc., 305, Bic Drive, Milford, CT 06460, USA*

The principles of rapid solidification technology were applied to cause dispersion strengthening in the intermetallic niobium aluminide ($NbAl_3$). Two niobium aluminide compositions, $NbAl_3$ and $NbAl_3$ containing 1% $TiB_2$ were prepared as rapidly solidified powders by an advanced melt spinning–pulverization technique. Powders were consolidated by hot isostatic pressing (HIP). HIPed materials were characterized for microstructures and high-temperature deformation behaviour. The microstructure of the HIPed niobium aluminides consisted of a recrystallized grain structure with grain size in the range of 5–10 μm. As HIPed $NbAl_3$ + 1% $TiB_2$ material additionally exhibited the presence of multiple phases in a finely dispersed state. The grain boundaries in this material were populated by 1–2.5 μm particles of intermetallic phase identified as $Nb_3Al_2$ with a hexagonal crystal structure, while 0.1–0.2 μm sized dispersoids of a NbB-base phase with orthorhombic crystal structure formed in the interior of the grains. The flow characteristics of the niobium aluminide materials were investigated by constant-velocity compression testing at 1300 and 1477 K with strain rates ranging between $10^{-2}$ and $10^{-6}\,s^{-1}$. $NbAl_3$ + 1% $TiB_2$ alloy containing a dispersion of second phases, notably borides, showed superior strength compared with the baseline $NbAl_3$ composition. This suggests possible interaction of the grain boundaries and dislocation with the second-phase particles (i.e. borides).

## 1. Introduction

New approaches are currently being sought by materials scientists to develop and characterize advanced high-temperature structural intermetallic materials and composites. These materials would find potential aircraft applications in the temperature range 2000–3000 °F ( ~ 1093–1649 °C) in advanced gas turbine engines. Many ordered intermetallic compounds appear to have great potential for applications as high-temperature structural materials because of their high melting points and stability in oxidizing environments.

The candidate intermetallics for advanced elevated temperatures include the aluminides of nickel, titanium and niobium. Over the past several years, a considerable amount of work has been performed to understand the room temperature and elevated temperature mechanical properties of intermetallic alloys based on aluminides with the majority of research efforts concentrating on the high-temperature creep behaviour and low-temperature fracture toughness [1–6]. Various approaches are being investigated based on particulate composite [7, 8], and unidirectional fibre reinforcement [9] to enhance high-temperature strength of intermetallics. Recently, studies are underway to develop "dispersion strengthened" intermetallic alloys using the principles of rapid solidification technology (RST) [10–12]. The emphasis in this case is to disperse a low volume fraction (< 5%) of thermodynamically stable materials such as HfC, $TiB_2$ and $HfB_2$ as ultrafine dispersoids (~ 30 nm sized) uniformly throughout the matrix of the intermetallic materials. These dispersoid additions have resulted in behaviour similar to that of oxide dispersion strengthened (ODS) alloys, for example, high stress exponents, departure side pinning of dislocations to particles and probable threshold stresses for creep. Another beneficial effect of RST is to impart fine-grained structure to the matrix of the alloys stabilized by fine dispersoids. Low-temperature ductility improvement has been noticed in otherwise brittle polycrystalline NiAl by refining the grains to sizes smaller than a critical value [13].

$NbAl_3$ is one of the three intermetallic compounds formed in the niobium–aluminium system. It has no detectable homogeneity range, melts congruently and has the $DO_{22}$ crystal structure, similar to $TiAl_3$. Niobium aluminides are difficult to process, and due to their intrinsic brittleness, the niobium aluminide ingots crack during cooling. Powder metallurgy (PM) processing appears to be a potential technique to process these alloys, circumventing the problems associated with brittleness. In this report, we describe the microstructures and elevated-temperature mechanical properties of rapidly solidified $NbAl_3$ containing $TiB_2$ as a dispersion-strengthening agent.


0022–2461 

## 2. Experimental procedure

$NbAl_3$ intermetallic alloys containing 0–1 wt % $TiB_2$ were prepared as prealloyed ingots from high purity ($\geqslant 99.9\%$) constituent elements by the non-consumable arc-melting process under an argon atmosphere. The ingots were repeatedly melted to ensure good chemical homogeneity. The prealloyed $NbAl_3$ and $NbAl_3 + 1\%$ $TiB_2$ ingots were rapidly solidified as melt-spun filaments using an advanced melt-spinning technique. Because the melting point of $NbAl_3$ is rather high, most rapid solidification processes involving ceramic crucibles will suffer from a reaction between the crucible material and the melt. The advanced melt-spinning process employed involves skull melting the alloy in a water-cooled cold hearth by a non-consumable tungsten arc. Rapid solidification was achieved by extracting thin filaments from the melt by means of a fast rotating molybdenum wheel. The rapidly solidified filaments, typically 20–50 μm thick and 0.5 mm wide were pulverized into powders (below 40 mesh particle size) by a rotating hammer mill under an inert gas environment. The powders were consolidated to full density in titanium cans by the method of hot isostatic pressing at 2550 °F (~ 1399 °C) and $15 \times 10^3$ p.s.i. pressure ($10^3$ p.s.i. $= 6.89\ N\,mm^{-2}$).

Compression tests were carried out to determine the flow stress and strain-rate sensitivity of $NbAl_3$ materials. Tests were conducted at 1300 and 1477 K under an inert gas environment. Test specimens were 5 mm diameter and 10 mm high, and tests were carried out on an Instron machine with specimen temperature variations within $\pm 1$ K. Boron nitride lubrication was used with alumina compression platens for this work, and the extent of barrelling was found to be relatively small even after a true strain level of 0.3. Strain rates were maintained constant during tests by continuously decreasing crosshead velocity in an exponential manner as the specimen height decreased during the test. The true stress, σ, was calculated by dividing load, $P$, from the chart, by the instantaneous cross-sectional area, $A$, assuming volume constancy. The relevant relationships are

$$\varepsilon = \dot{\varepsilon} \times \text{time} \quad (\dot{\varepsilon} \text{ is negative}) \tag{1}$$

$$A = A_0 e^{-\varepsilon} \tag{2}$$

$$\sigma = P/A \tag{3}$$

where ε is the true compression strain.

The microstructure of the alloy was characterized by optical metallography, scanning electron microscopy (SEM), transmission electron microscopy (TEM) and X-ray diffraction (XRD) analyses. Samples for optical and SEM metallography were etched with a solution of 33% $HNO_3$–33% $CH_3COOH$. Samples for TEM studies were prepared by cutting 250 μm thick discs, mechanically grinding to about 100 μm and electropolishing in a 10% perchloric acid–methanol solution. Some specimens were also prepared by direct milling to prevent possible formation of hydrides during polishing. The microstructures of the specimens prepared by both methods were, however, comparable.

## 3. Results and discussion

### 3.1. Microstructures of rapidly solidified $NbAl_3$ and $NbAl_3 + 1TiB_2$ alloy

Fig. 1 shows an optical photomicrograph of a transverse section of the HIPed bar of $NbAl_3$. Figs 2 and 3 show typical scanning electron micrographs of the as-HIPed $NbAl_3$ and $NbAl_3 + 1TiB_2$, respectively. A recrystallized microstructure with equiaxed grains in the 5–10 μm range is observed in the niobium aluminide materials. The microstructure of $NbAl_3 + 1$ $TiB_2$ material shows a dispersion of additional phase(s) in the $NbAl_3$ matrix.

X-ray diffraction analysis was conducted to determine the crystal structure of the phases present in the $NbAl_3 + 1$ $TiB_2$ material. The major peaks of the diffraction scan were identified to arise from the tetragonal $Al_3Nb$ phase ($a = 0.38$ and $c = 0.86$ nm). In addition to the major peaks, a few minor peaks

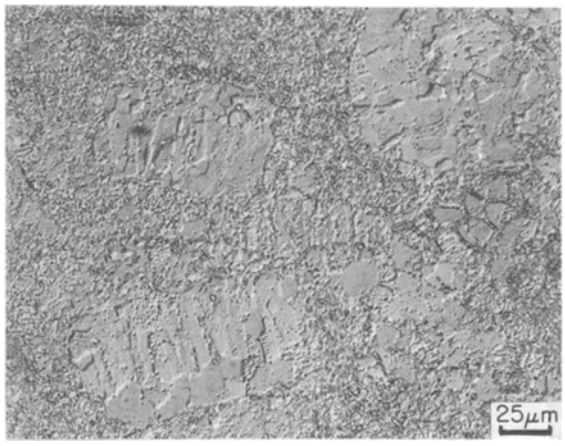


*Figure 1* Optical photomicrograph of transverse section of HIPed $NbAl_3$ bar.

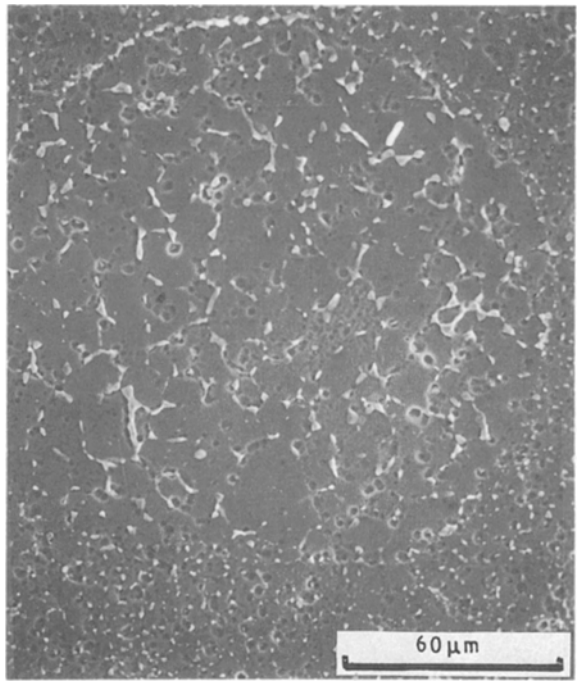


*Figure 2* Scanning electron micrograph of HIPed $NbAl_3$.

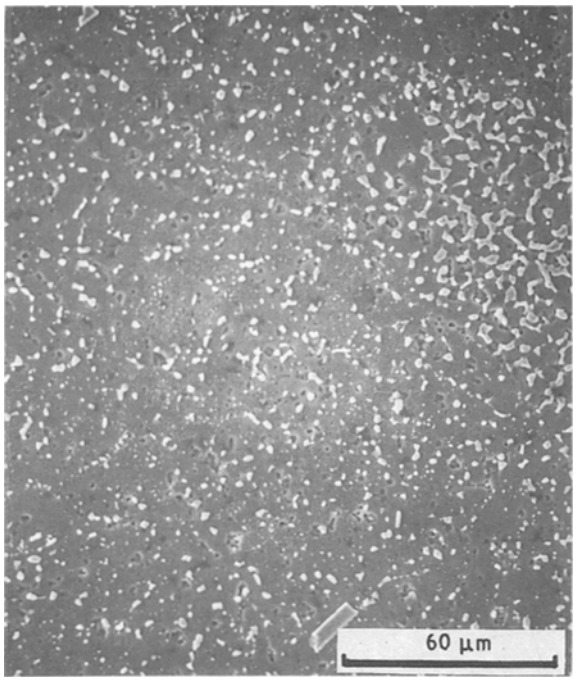


*Figure 3* Scanning electron micrograph of HIPed $NbAl_3$ + 1% $TiB_2$.

were also observed. These peaks could not be identified with any phase known to form in the Al–Nb system. Therefore, further analysis of the secondary phases was carried out in the TEM.

TEM studies showed that the $NbAl_3$ + 1 $TiB_2$ material consisted of equiaxed grains of the matrix with a uniform distribution of second-phase particles. The size of the matrix grains ranged from 2–10 μm while the second phase particles ranged in size from about 0.1–2.5 μm. Most of the coarse particles formed at the triple points of the matrix grains and the finer particles within the grains, Fig. 4.

X-ray microanalysis and electron energy loss spectroscopy (EELS) were performed to characterize the chemistry of the phases. *k* factors for X-ray microanalysis were determined from independent Nb–Ti and $Ti_3Al$ binary standards and the peak intensities corrected for absorption prior to quantification. Energy dispersive spectra of the matrix phase showed peaks from aluminium and niobium, Fig. 5. Quantitative analysis established chemistry of the matrix phase to be 24.5 (1.5) Al, 74.1 (0.7) Nb, 0.8 (0.1) Ti and 0.3 (0.1) Cr* in agreement with $NbAl_3$ stoichiometry. The residual elements, such as titanium and chromium are proposed to substitute for niobium.

EDS analysis also indicated the presence of two types of second phase particles in the alloy. The coarse particles, which populated the grain boundaries, were rich in aluminium and niobium, Fig. 6a, and their Nb/Al ratio was higher than that observed for the matrix phase. These particles also contained slightly increased concentrations of residual chromium and titanium. No oxygen peak was observed indicating that the particles were not oxides. In order to examine the presence of other lighter elements, EELS analysis

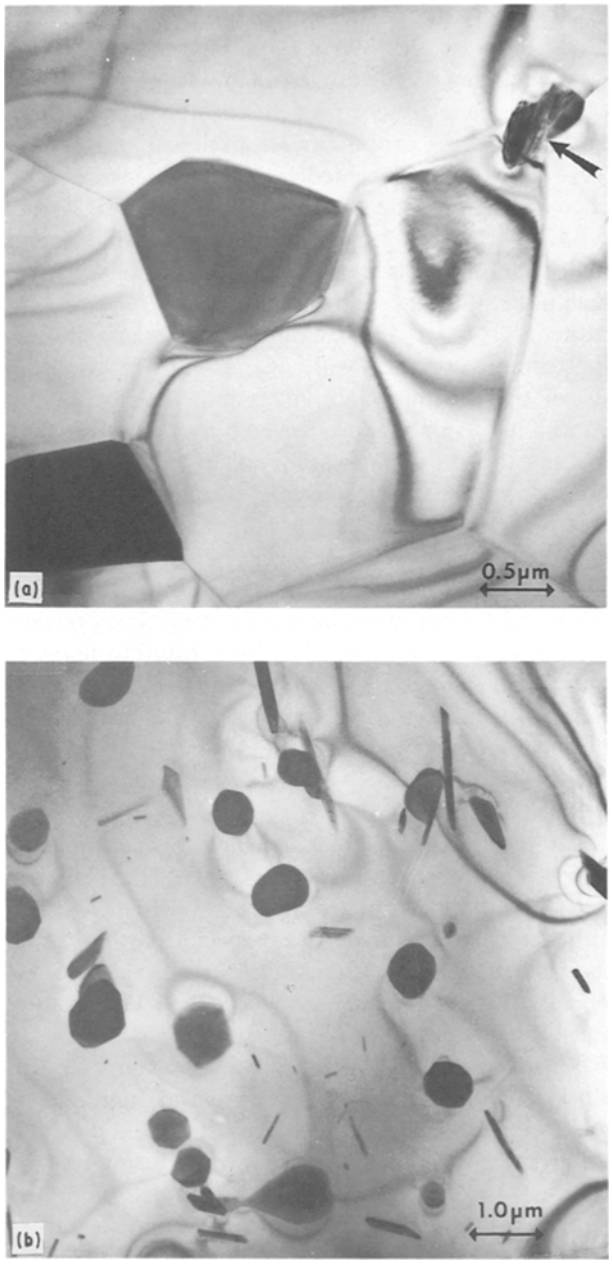


*Figure 4* Typical bright-field TEM image of as-HIPed $NbAl_3$ + 1% $TiB_2$ showing second-phase precipitates (a) at the grain boundaries and (b) inside the grains.

was conducted. The analysis revealed that the coarse Al–Nb particles did not contain boron, Fig. 6b. Quantitative analysis of the Al–Nb particles based on the heavy elements established a chemistry of (at %) 40.5 (1.8) Al, 55.2 (1.2) Nb, 2.2 (0.3) Ti and 1.2 (0.2) Cr. Allowing for substitution of chromium and titanium for niobium, the chemistry of the phase was reasonably close to a $Nb_3Al_2$ stoichiometry.

Occasionally, smaller particles containing only niobium were also observed inside the grain bodies (arrowed in Fig. 4). The particles were smaller, typically ranging from 0.1–0.2 μm and showed some degree of faulting. EDS and EELS analyses showed that the niobium rich particles contained a high concentration of boron suggesting that they could be niobium boride (Fig. 7).

* Numbers in parenthesis are error bars (1σ SD).

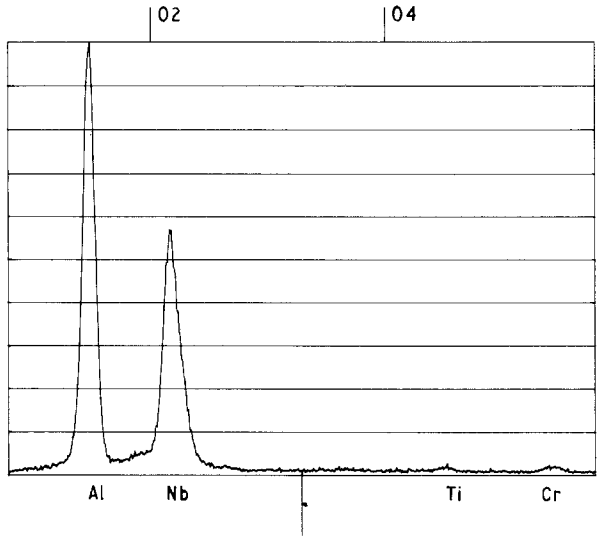


*Figure 5* EDS spectrum of the matrix phase in the $NbAl_3$ + 1% $TiB_2$ specimen of Fig. 4.

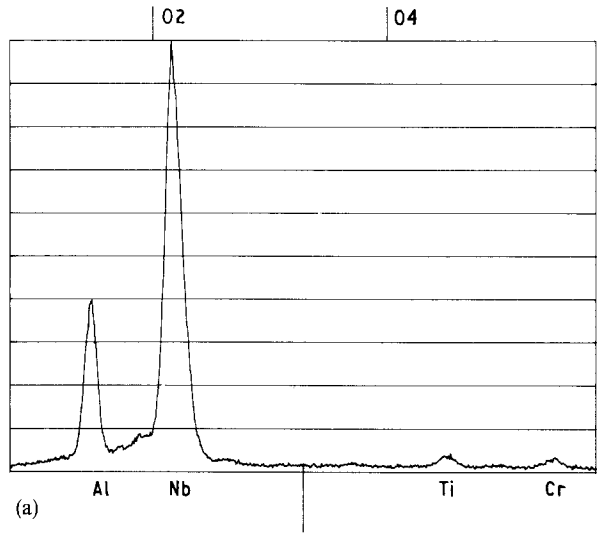


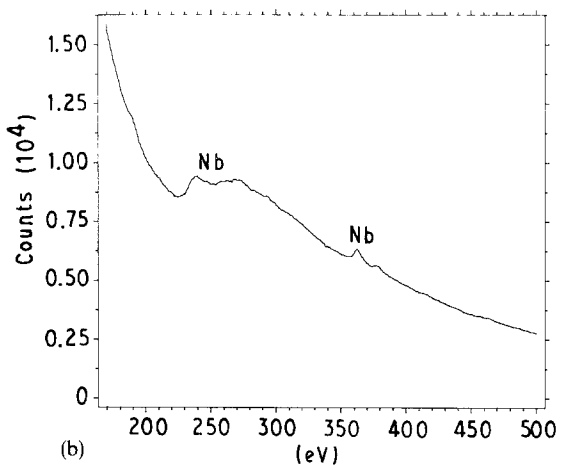


*Figure 6* (a) EDS spectrum of the coarse grain-boundary precipitates in $NbAl_3$ + 1% $TiB_2$ specimen of Fig. 4. (b) EELS spectrum of the coarse grain-boundary precipitates in $NbAl_3$ + 1% $TiB_2$ specimen of Fig. 4. Note the absence of boron in the spectrum.

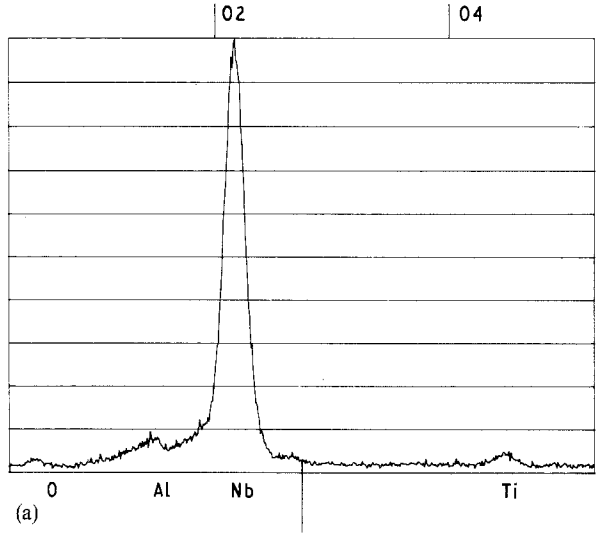


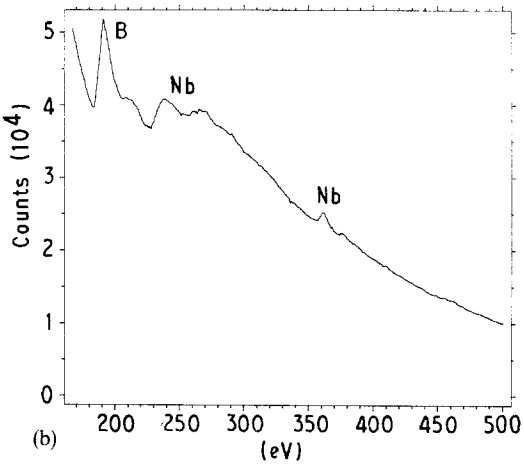


*Figure 7* (a) EDS spectrum from the small precipitates inside the grains of $NbAl_3$ + 1% $TiB_2$ specimen (indicated by arrow in Fig. 4). A strong niobium peak is noticed. (b) EELS spectrum from the small precipitates inside grains of $NbAl_3$ + 1% $TiB_2$ specimen of Fig. 4. Notice the presence of niobium and boron.

Convergent beam electron diffraction (CBED) analysis was conducted to identify the phases present in the sample. Fig. 8 shows a [0 0 1] diffraction pattern from the matrix phase. The four-fold pattern symmetry, unit cell dimensions and the extinctions were in agreement with the tetragonal structure and spacegroup (I4/mmm, no. 139) published for the $NbAl_3$ phase. CBED studies determined the structure of the $Nb_3Al_2$ second-phase coarse particles to be hexagonal. Fig. 9 is a [0 0 0 1] pattern from the particle showing six-fold symmetry. Based on the pattern symmetry, reflections in the zero and the diameter of the first-order Laue zone, the unit cell dimensions of the hexagonal phase were determined to be $a = 0.76$ and $c = 0.52$ nm, with a possible spacegroup of $P6_3/mcm$ for the phase. The details of the crystallographic analysis of the phases is described in a further publication [14]. Diffraction analysis of the small niobium-rich particle, Fig. 10, identified their crystal structure to be orthorhombic with unit cell dimensions of $a = 0.33$, $b = 0.87$ and $c = 0.32$ nm (spacegroup: Cmcm no. 63). Based on the structure, the particles were identified to be NbB [15].

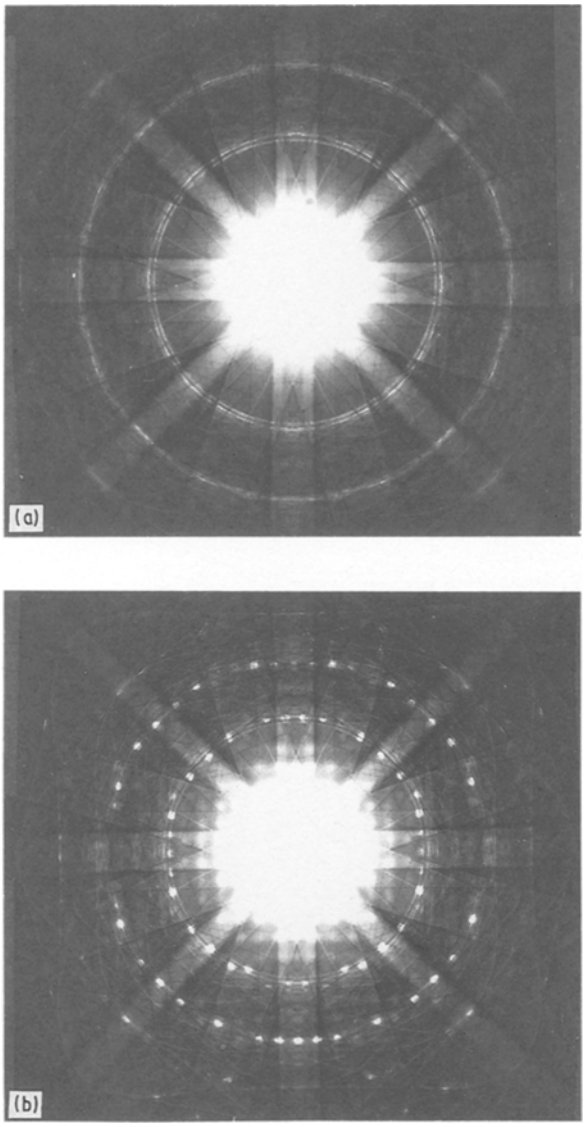


*Figure 8* [001] Convergent beam diffractions pattern from the matrix phase of $NbAl_3$ + 1% $TiB_2$ specimen showing four-fold symmetry; patterns taken with (a) large C2 aperture and (b) small C2 aperture.

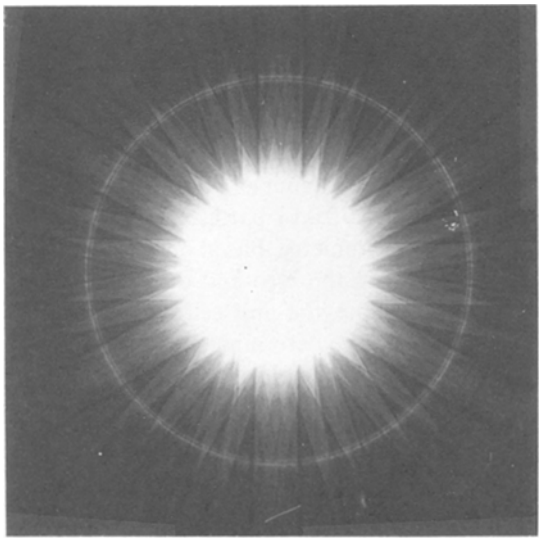

*Figure 9* [0001] Diffraction pattern of the coarse second-phase particles at the grain boundaries of $NbAl_3$ + 1% $TiB_2$ alloys as shown in Fig. 4.

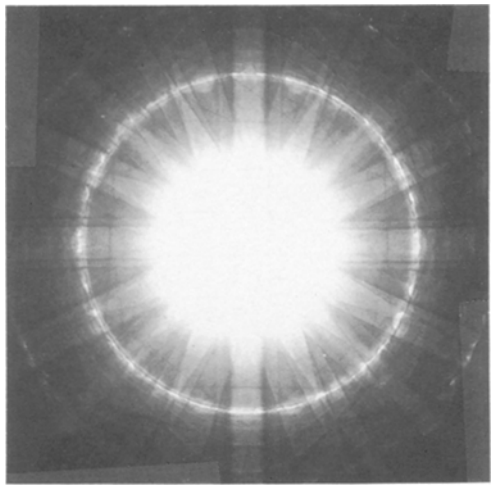

*Figure 10* [0 1 0] CBED pattern from the small NbB particles inside the grains of the $NbAl_3$ + 1% $TiB_2$ alloy as shown in Fig. 4.

The results of the TEM studies demonstrated that the structure of the alloy consisted essentially of a dispersion of second-phase intermetallic particles in an $NbAl_3$ matrix. It is not clear if the second "$Nb_3Al_2$" phase observed in the present study originates from the Nb–Al binary system or is a phase introduced from the Nb–Al–Cr or Nb–Al–Ti ternary systems. Because published phase diagrams for the Nb–Al binary system do not indicate a $Nb_3Al_2$ compound, further work is required to clarify this issue.

## 3.2. Mechanical properties

Fig. 11 shows the compressive true stress–true strain data of $NbAl_3$ and $NbAl_3$ + $1TiB_2$ alloys at 1477 K. A few observations are as follows.

At higher strain rates ($10^{-2}\,s^{-1}$), the compression test specimens failed immediately or after a small strain at 1477 K, possibly because the flow stress exceeded the grain-boundary fracture strength. At intermediate strain rate ($10^{-3}\,s^{-1}$), specimens showed a diffuse yielding over 2%–3% strain followed by negative strain hardening. As the strain rate decreased (i.e. to $10^{-4}\,s^{-1}$), there was a tendency toward a steady state behaviour.

The hot compression tests data on $NbAl_3$ and $NbAl_3$ + 1 $TiB_2$ alloys carried out at 1300 K are shown plotted in Fig. 12. At strain rates, $10^{-4}\,s^{-1}$ and $10^{-5}\,s^{-1}$, both the materials showed diffused yielding followed by strain softening. At slower rate of $10^{-6}\,s^{-1}$, deformation took place in the materials at constant flow stress after a small amount of work hardening.

Steady state compression flow stress versus strain rate plots for $NbAl_3$ and $NbAl_3$ + $1TiB_2$ on a log–log scale are given in Figs 13 and 14. The corresponding strain rate sensitivity, $m$, values for the two alloys at the two temperatures examined are given in Fig. 15. The data points in this plot are fitted with the best least-square polynomials. $NbAl_3$ + $1TiB_2$ alloy containing a dispersion of boride phase shows superior strength compared to the baseline $NbAl_3$ alloy. This suggests that some interaction of the grain boundaries

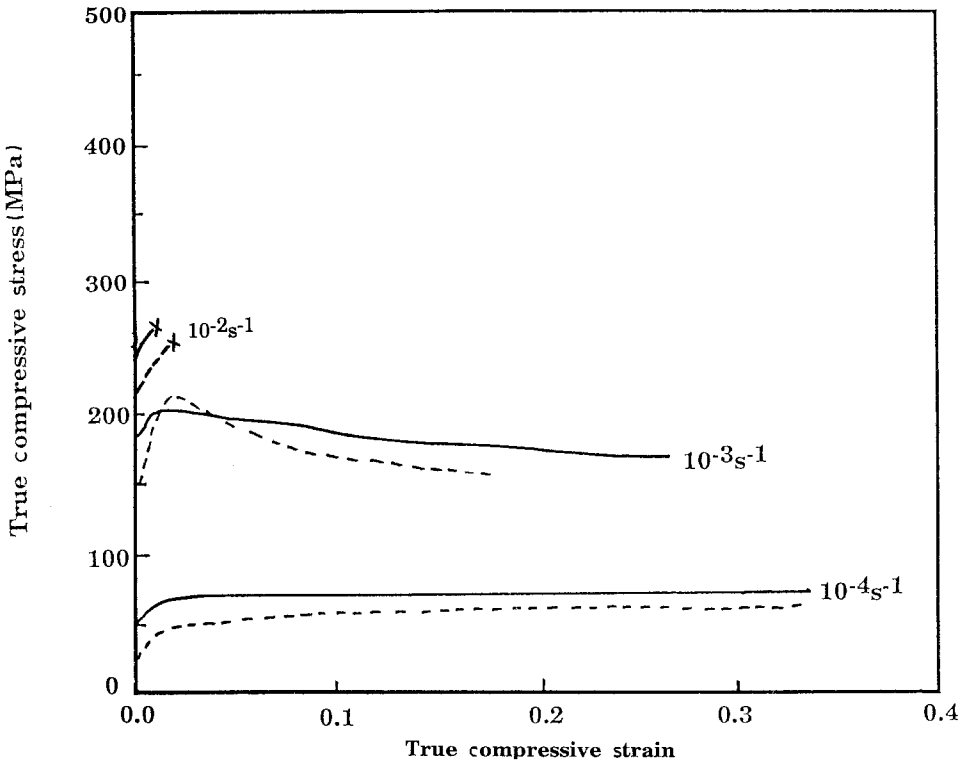


*Figure 11* Flow stress–strain behaviour of (---) as-HIPed $NbAl_3$ and (——) $NbAl_3$ + 1% $TiB_2$ at 1477 K.

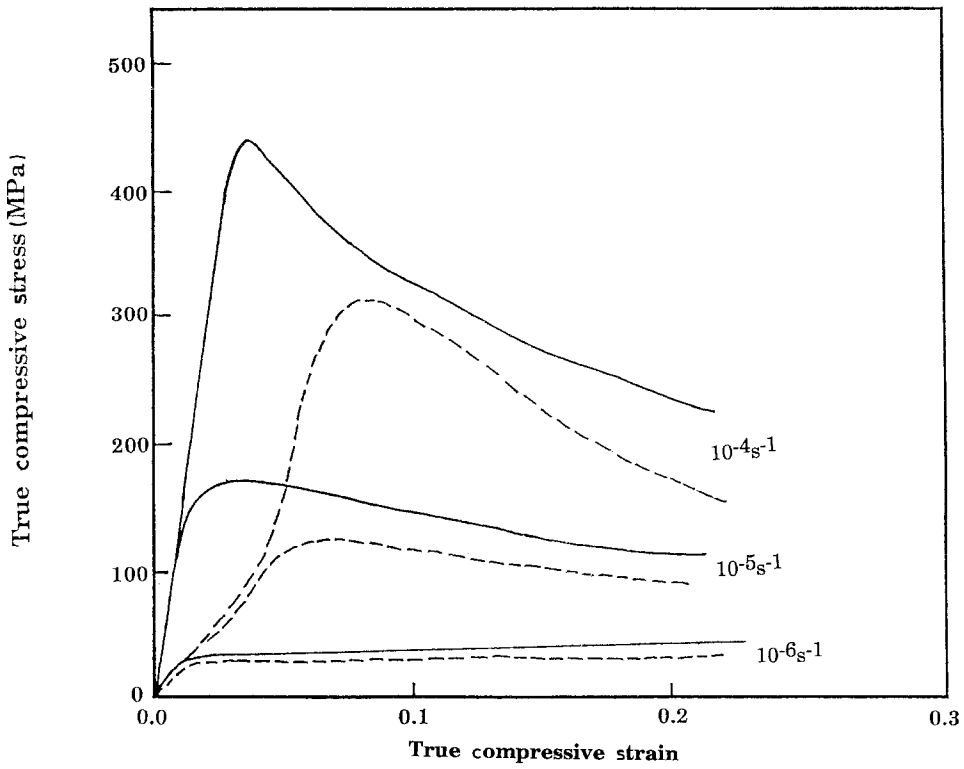


*Figure 12* Flow stress–strain rate behaviour of (---) as-HIPed $NbAl_3$ and (——) $NbAl_3$ + 1% $TiB_2$ at 1300 K.

or dislocations with the second-phase particles (i.e. borides) is occurring. This could give rise to the development of a particle-pinned fine grain structure. In the event, some diffusional creep processes are occurring at this temperature, the other possible component of hardening can occur from coarsening of the sub-structure with continued deformation.

Figs 13 and 14 are stress–strain rate plots of the rapidly solidified $NbAl_3$ series alloys of the present investigation compared with the plots of the rapidly solidified NiAl alloys [12]. Over the range of strain rates and temperatures examined, the $NbAl_3$ alloys showed improved strength compared to NiAl alloys.

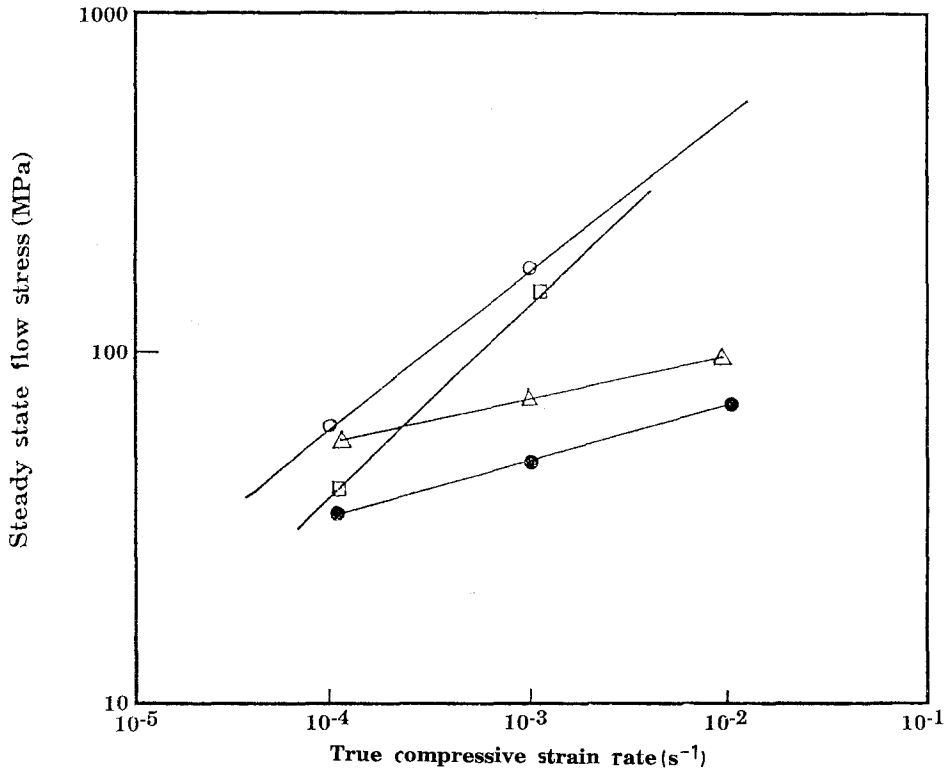


*Figure 13* Flow stress–strain rate data of $NbAl_3$ group materials compared to NiAl group materials at 1477 K. (○) $NbAl_3$ + 1% $TiB_2$, (□) $NbAl_3$, (△) NiAl + 4% HfC, (●) NiAl.

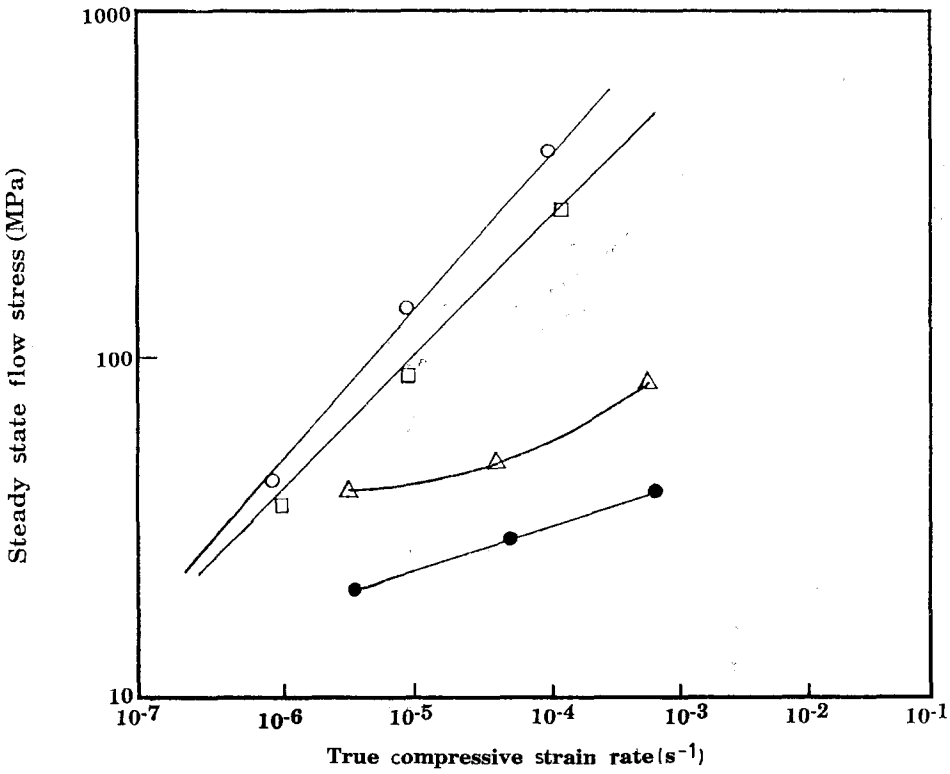


*Figure 14* Flow stress–strain rate data of $NbAl_3$ group materials compared to NiAl group materials at 1300 K. (○) $NbAl_3$ + 1% $TiB_2$, (□) $NbAl_3$, (△) NiAl + 4% HfC, (●) NiAl.

The significantly high $m$ values (0.4–0.65) for the $NbAl_3$ materials compared to the $m$ values (0.2–0.25) of NiAl alloys [12] suggest possibly fine grain structures of the niobium aluminides produced by RST. Fine grain structures created in niobium aluminides via RST remain stable even after thermal exposure at considerably high temperatures during hot consolidation. Such fine grain structures hold great promise from a standpoint of ease in hot processing these intermetallic materials.

## 4. Conclusion

Rapid solidification has been employed to create unique microstructures that are not possible through conventional ingot metallurgy processing. In the present work, advanced rapid solidification technology

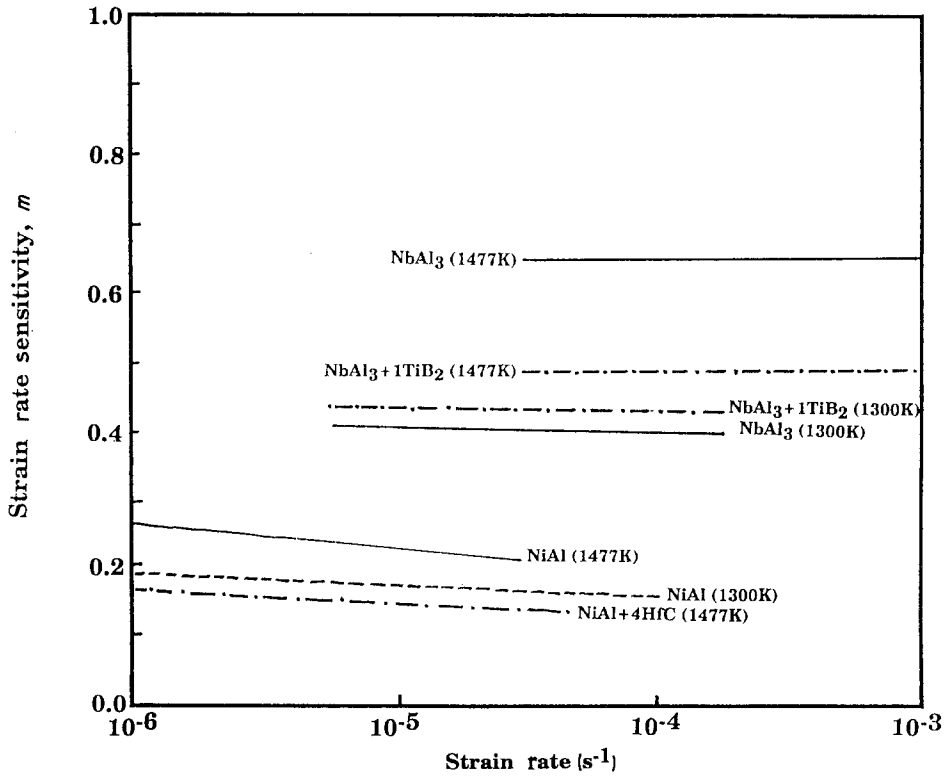


*Figure 15* The $m$ values as a function of strain rate for various $NbAl_3$ group materials as compared to various NiAl group materials.

has been utilized to create fine-grained structures in $NbAl_3$ matrix with a uniform dispersion of stable second-phase particles. The reason for formation of the intermetallic $Nb_3Al_2$ phase in the present materials as somewhat coarse precipitate particles at the grain boundaries of the $Nb_3Al$ matrix phase, is not clear. The stoichiometry of the $NbAl_3$ and the alloying additions to it need to be controlled closely during processing to avoid formation of the second intermetallic phase particles with undesirable particle size and distribution.

The second-phase particles, especially borides, remain fine (0.1–0.2 μm) even after hot processing the alloys at considerably high temperatures up to 2550 °F ( ~ 1399 °C). The high-temperature strength of $NbAl_3$ is improved by incorporation of second-phase particles based on borides via RST. It might be possible to incorporate a higher volume fraction of boride or similar stable phases as incoherent dispersoids in the $NbAl_3$ matrix than the present $NbAl_3$ + $1TiB_2$ alloy. A large volume fraction of ultrafine incoherent particles with low interfacial energies and large elastic misfits would be stable against coarsening due to Ostwald ripening. If a large volume fraction of ultrafine dispersoid can be formed in $NbAl_3$-type intermetallic materials via the route of RST, the particles will be expected to be extremely closely spaced, the concentration of solutes in the vicinity of the particles and surrounding matrix will tend to equalize, minimizing the solute concentration gradients between the particles, and hence the growth of the particles will be retarded. The presence of fine dispersoids in sufficient volume fraction will lead to higher dislocation density between subgrains during creep. The particles will furthermore anchor subgrains leading to finer substructure. These factors can yield an increased creep resistance of the materials.

The high strain rate sensitivity values (0.4–0.6) calculated from the compression tests on $NbAl_3$ materials show that deformation at high temperature occurs by diffusional creep (Coble creep) with significant dislocation climb and grain-boundary migration.

## Acknowledgement

The present work was carried out under a Contract F33615-89-C-5641 from the Materials Laboratory of Wright Patterson Air Force Base, OH, USA.

## References

1. D. M. DIMIDUK and D. B. MIRACLE, *Mater. Res. Soc. Proc.* **133** (1989) 348.
2. L. CHRISTODOULOU, P. A. PARRISH and C. R. CROWE, *MRS Symposium Proceedings* Vol. **120** (MRS, Pittsburgh, PA, 1988) 29.
3. C. T. LIU, A. L. TAUB, N. S. STOLOFF and C. C. KOCH, (eds), "High Temperature Ordered Intermetallic Alloys III", *MRS Symposium Proceedings*, **133** (MRS, Pittsburgh, PA, 1988).
4. H. C. CAO, B. J. DALGLEISH, H. E. DEVE, C. ELLIOTT, A. G. EVANS, R. MEHRABIAN and G. R. ODETTE, *Acta Metall.* **37** (1989) 2969.
5. D. L. ANTON, D. M. SHAH, D. N. DUHL and A. F. GIAMEI, *J. Metals* **41** (1989) 12.
6. F. D. LEMKEY, S. G. FISHMAN, A. G. EVANS and J. R. STRIFE, (eds), "High Temperature High Performance Composites", *MRS Symposium Proceedings*, **120** (MRS, Pittsburgh, PA, 1988).
7. J. D. WHITTENBERGER, S. K. MANNAN and K. S. KUMAR, *Scripta Metall.* **23** (1989) 2055.
8. J. D. WHITTENBERGER, D. J. GAYDOSH and K. S. KUMAR, *J. Mater. Sci.* **25** (1990) 35.

9. M. V. NATHAL, R. D. NOEBE, I. E. LOCCI, S. L. DRAPER and D. J. GAYDOSH, "Hitemp review", NASA Conference Publication 10025, (NASA Lewis Research Center, Cleveland, OH, 1988) p. 235.
10. S. C. JHA and R. RAY, *J. Mater. Sci. Lett.* **7** (1988) 285.
11. S. C. JHA, R. RAY and D. J. GAYDOSH, *Scripta Metall.* **23** (1989) 805.
12. S. C. JHA, R. RAY and J. D. WHITTENBERGER, *Mater. Sci. Eng.* **A119** (1989) 103.
13. E. M. SCHULSON and D. R. BARKER, *Scripta Metall.* **17** (1983) 519.
14. R. AYER and R. RAY, *Met. Trans.* **22A** (1991) 1901.
15. P. VILLARS and L. D. CLAVERT, "Pearson's Handbook of Crystallographic Data for Intermetallic Phases", *American Society of Metals*, Metals Park, OH, 1985).

*Received 14 November 1990*
*and accepted 20 February 1991*